Physiochemical properties and antibacterial activity of silver nanoparticles green synthesized by *Camellia sinensis* and *Prunus africana* extracts

Kenneth Ssekatawa
College of Veterinary Medicine Animal Resources and Biosecurity, Makerere University P. O. Box 7062 Kampala Uganda
Denis Byarugaba
College of Veterinary Medicine Animal Resources and Biosecurity, Makerere University P. O. Box 7062 Kampala Uganda
Charles Kato
College of Veterinary Medicine Animal Resources and Biosecurity, Makerere University P. O. Box 7062 Kampala Uganda
Eddie Wampande
College of Veterinary Medicine Animal Resources and Biosecurity, Makerere University P. O. Box 7062 Kampala Uganda
Francis Ejobi
College of Veterinary Medicine Animal Resources and Biosecurity, Makerere University P. O. Box 7062 Kampala Uganda
Jesca Nakavuma
College of Veterinary Medicine Animal Resources and Biosecurity, Makerere University P. O. Box 7062 Kampala Uganda
Malik Maaza
UNESCO-UNISA Africa Chair in Nanosciences/Nanotechnology, College of Graduate Studies, University of South Africa (UNISA), Muckleneuk Ridge, PO Box 392, Pretoria, South Africa
Juliet Sackey
Nanosciences African Network (NANOAFNET), iThemba LABS-National Research Foundation, Old Faure Road, 7129 Somerset West, South Africa
Edward Nxumalo
University of South Africa-Florida Campus Private Bag X6 Florida 1710
John Kirabira (kirabirajb@gmail.com)
African Center of Excellence in Materials, Product Development and Nanotechnology, College of Engineering, Design, Art and Technology, Makerere University P. O. Box 7062, Kampala Uganda

Research Article

Keywords: Green synthesis, silver nanoparticles, antibiotic resistance, Prunus africana, Camellia sinensis

Posted Date: January 21st, 2021

DOI: https://doi.org/10.21203/rs.3.rs-143995/v1

Abstract

Antibiotics have been the nucleus of chemotherapy since their discovery and introduction into the healthcare system in the 1940s. They are used routinely not only to treat bacterial infections but also to prevent infections in patients with compromised immune systems and enhancing growth in livestock. However, resistance to last-resort antibiotics used in the treatment of MDR infections has been reported worldwide. Therefore, the aim of this study was to evaluate green synthesized nanomaterials such as AgNPs as alternatives to antibiotics. UV Vis Spectroscopy surface plasmon resonance peaks for AgNPs were obtained between 417 to 475nm. XRD analysis generated 4 peaks for both PAE and CSE biosynthesized AgNPs positioned at 2θ angles of 38.2˚, 44.4˚, 64.5˚, and 77.4˚ corresponding to crystal planes (111), (200), (220) and (311) respectively. DLS registered mean zeta potential of + 6.3mV and + 0.9mV for PAE and CSE biosynthesized nanoparticles respectively. FTIR spectra exhibited bands corresponding to different organic functional groups confirming capping of AgNPs by PAE and CSE phytochemicals. FESEM imaging showed that AgNPs were spherical with average size distribution ranging from 10 to 19nm. Biosynthesized AgNPs exhibited maximum growth inhibitory zones of 21mm with MIC and MBC of 125µg/ml and 250µg/ml respectively against carbapenem resistant bacteria.

Introduction

The greatest challenge of our generation and generations to come is antimicrobial resistance as different pathogenic bacteria have continuously evolved to become resistant to even the most recently synthesized antibiotics. This scenario has complicated treatment outcomes even to the commonest bacterial infections (Livermore et al., 2011). The U.S. Centers for Disease Control and Prevention (CDC) approximates that antibiotic resistance is accountable for more than 2 million infections and 23,000 deaths each year in the United States, at a direct cost of $20 billion and extra output losses of $35 billion (CDC, 2013). In Europe, an estimated 25,000 deaths are attributable to antibiotic resistant infections, costing €1.5 billion annually in direct and indirect costs (ECDC., 2017). Even though there is no trustworthy data on economic losses in the third world countries, Studies in India (Laxminarayan, Boeckel, & Teillant, 2015), Tanzania and Mozambique (Kayange, Kamugisha, Mwizamholya, Jeremiah, & Mshana, 2010; Roca et al., 2008) point out that increased deaths in neonates are attributed to antibiotics resistant infections.

Repeated attempts to develop alternative approaches such as use of herbal medicines; fish mucins and nanotechnology have been made. Of all, the most promising novel therapeutic option in this present scenario is the application of nano-scale materials as antimicrobial agents as they have exhibited very high surface area to volume ratio and the exceptional chemical complexities.

The nanotechnology field is anticipated to be the gate way in combating both infectious and non-infectious diseases (Albrecht, Evans, & Raston, 2006; Morones et al., 2005). Among the metallic nanoparticles, Silver nanoparticles (Ag NPs) owing to their potent antimicrobial activity against multidrug resistant pathogens ranging from viruses, prokaryotes to eukaryotes, have become the center of attention of robust research (Gong et al., 2007). Silver NPs exhibited great antibacterial efficacy against *Vibrio cholera, Salmonella typhi Staphylococcus aureus, Escherichia coli* and *Pseudomonas aeruginosa* in previous experiments (W.-R. Li et al., 2010; Morones et al., 2005). In the 1960s and 70s, a combination of silver nitrate and sulfonamide to form silver sulfadiazine cream with broad-spectrum antimicrobial activity was the first option for topical treatment of burns as its efficacy against *E. coli, S. aureus, Klebsiella sp*., and *Pseudomonas sp*. fungal and viral infections was laudable (Fox & Modak, 1974; Moyer, BRENTANO, GRAVENS, MARGRAF, & MONAFO, 1965). However, Nanoscale Silver in comparison to non-nanoscale one such as silver nitrate, presents concurrently high solubility, great chemical reactivity, and formidable broad-spectrum bacteria growth inhibitory activity at very low concentration (Agnihotri, Mukherji, & Mukherji, 2013; Bondarenko et al., 2013; Martinez-Gutierrez et al., 2013; Panáček et al., 2006). Most importantly, the bactericidal action of nanoparticles is reliant on physicochemical properties such as size and shape hence variability in the mode of action of different forms of nanoparticles may enlighten why resistance to this treatment is yet to be reported (Kvítek et al., 2008; Marková et al., 2012). To date, the bactericidal effect of nanoparticles (NP) is yet to be fully clarified. However, it might reside within the capacity of nanoparticles to discharge cations from nano-prearranged surfaces, which irreversibly disorganize bacterial cell wall, inactivate vital proteins, chelate DNA and lead to generation of reactive oxygen species known to have high microbicidal activity (N. Durán, Nakazato, & Seabra, 2016; Rizzello, Cingolani, & Pompa, 2013; Wang, Hu, & Shao, 2017; Yin et al., 2020).

Furthermore, the conventional approaches employed to fabricate nanoparticles such as chemical and physical methods have limitations. Physical approaches are not cost effective because they regularly require extremely expensive equipment, high temperature and pressure in addition to high energy consumption (Guzmán, Dille, & Godet, 2009) hence making them unpopular in third world countries. Chemo nanoparticle fabrication mainly entails the models of wet chemistry where several chemical reducing agents are exploited to reduce metal salts in solutions (Polavarapu & Liz-Marzán, 2013; Tahir et al., 2013). The main drawbacks faced by chemical methods include use of costly metal salts in addition to hazardous solvents and reducing agents. Therefore, nanoparticles synthesized by chemical methods exhibit nonselective toxic to both target bacterial and host cells (Kawata, Osawa, & Okabe, 2009). Additionally, numerous stabilizers are also necessary to thwart aggregation of nanoparticles to make them physiologically compatible and functional (Castro, Blázquez, González, & Ballester, 2014).

Due to challenges faced by conventional methods used in fabrication of nanoparticles, researchers have been motivated to invent novel, cost effective, uncomplicated eco-friendly biological approaches. Several biological approaches such as biosynthesis of nanoparticles using bacteria (Dickson, 1999), fungi (Nelson Durán, Marcato, Alves, De Souza, & Esposito, 2005) and plant extracts (Huang et al., 2007) have been reported. The most robust and popular of all is green synthesis of inorganic nanoparticles exploiting green plant extracts with antioxidant activity. The antioxidant properties of phenolic phytochemical are mainly attributed to their reducing abilities that permit them to operate as reducing agents and singlet oxygen scavengers, therefore reducing metal salts to nanoscale by scavenging electron from them. Presently possible sources of phytochemicals have been broadly studied in various plant species and plant parts including leaves, vegetables, fruits, oil seeds, herbs, barks, and roots, as well as in the extracts of entire plants (S. Li et al., 2007). Moreover, phytochemicals effectively support the green generation of nanoparticles by acting as reductants as well as functionalizing the resultant nanoparticles (Khan et al., 2013). Furthermore, the green based synthesis and functionalization of nanoparticles can be easily executed under normal physiological condition

(Huang *et al*., 2014). Without a doubt, due to the double effect of phytomolecules, green based synthesis meets the criteria of the best approach for preparing nanoparticles for biological applications because the resultant nanoparticles can be instantly applied without any post synthesis modification (Mie et al., 2014). This study examined the efficacy of *Camellia sinensis* and *Prunus africana* bark extract mediated green synthesized AgNPs against carbapenem resistant (CR) *E. coli* and *K. pneumoniae.*

Methods

Site description and source of materials

This study was carried out at the Pharmacology and Microbiology Laboratories, College of Veterinary Medicine, Animal Resources and Biosecurity, Makerere University, Materials Research Department (MRD), iThemba LABs, Cape Town and Nanotechnology Unit, department of Chemical Engineering, University of South Africa, Florida Campus. Processing of plants material, phytochemical extraction and green synthesis of Ag NPs were conducted from the Pharmacology laboratory and MRD while Ag NPs susceptibility assays were executed from the Microbiology Laboratory. Characterization of Nanoparticles was accomplished from MRD and Nanotechnology Unit. Confirmation of the identity of *Prunas africana* was done from department of Botany, Makerere University. Silver nitrate ($AgNO_3$) was obtained from Sigma Aldrich, USA, *Camelia sinensis* leaves were purchased from Igara Tea Estates, Bushenyi while *Prunas africana* bark and leaves were acquired from Maramagambo forest which covers the southern part of Queen Elizabeth National park located in Bushenyi district, Uganda.

Extraction of phytochemicals from *Camellia sinensis* and *Prunus africana*

Leaves of *Prunus africana* were analyzed by a botanist at department of Botany Makerere University to confirm its identity. To obtain *Camelia sinensis* extract (CSE) and *Prunas africana* extract (PAE), plant materials (leaves for CSE and the bark for PAE) were washed and lichens scrapped off, dried under shade on clean drying tables. The plant materials were then shredded into smaller particles 1-2cm^2 using knife and Pulverized into powdered form using electric laboratory grinder. Four hundred grams (400 g) of each powdered plant material were dissolved in 1.5L of sterile distilled de-ionized water in two different extraction bottles and left to stand for 5 days under darkness with daily occasional agitation for homogeneous mixing and extraction. The crude extract was sieved, and the filtrate concentrated by evaporation over steel pans in an oven at 37°C. After evaporation, the dry solid concentrate was scrapped off the pans, then transferred into clean top screw 50ml falcon tubes labeled as CSE and PAE and then stored 4°C.

Synthesis of silver nanoparticles using CSE and PAE

The Ag NPs were photosynthesized by adding 1ml (2%) of CSE concentrate into a round bottom flask containing 49 ml aqueous solution comprising 85mg of silver nitrate (0.5mM). The experiment was replicated to assess the effect of the concentration of plant extract on the yield and characteristics of nanoparticles by using different concentrations (4%, 8% and 16%) CSE. The above procedure was repeated using PAE, Table 1. UV Vis absorbance was taken immediately after mixing the plant extract and silver nitrate solution. For further absorbance reading, 5ml from each sample was dispensed into 15ml falcon tubes and kept in a dark cupboard. The round bottomed flasks were placed in a dark cabinet and left to stand for 24 hours, after which each was equipped with a magnetic stir bar and fixed with a cooling condenser. The reaction mixture was left to stand for 2 hours at 85°C, then left to cool down at room temperature followed by centrifuging at 9000 rpm for 30 minutes. The sediment obtained was washed numerous times with distilled de-ionized water after which the final precipitate produced was dried at 80°C in an oven for 12 hours.

Table 1:Concentration of plant extract, volume of plant extract and volume of silver nitrate used to green synthesize Ag NPs

Concentration of *Prunas africana* extract (%)	Volume of plant extract (ml)	Volume of Silver nitrate (ml)	Total volume (ml)
2	1	49	50
4	2	48	50
8	4	46	50
16	8	42	50

Characterization of silver nanoparticle.

UV–vis spectroscopy

This was achieved using a Cary 5000 UV Vis-NIR Spectrophotometer, Agilent Technologies. The samples were examined by UV–Vis spectroscopy operating at a resolution of 1nm between 190 and 800 nm ranges to analyze the optical property of biosynthesized Ag NPs. Absorbance was read at 0 minute, 0.5hr, 1hr, 2hr, 3hr 4hr and 5hr for the different concentrations of CSE-$AgNO_3$ solutions and at 0 minute, 0.5hr, 1hr, 2hr, 3hr, 4hr, 6hr, 8hr, 10hr, 12hr, 24hr and 72hr for PAE-$AgNO_3$ mixtures.

X-Ray diffraction Analysis (XRD)

About 500mg of green synthesized Ag NPs powder were analyzed with powder X-ray diffraction (XRD) employing BRUKER AXS diffractometer, D8 Advance (Germany) fitted with Cu-Ka radiation ($\lambda K\alpha_1$=1.5406Å) from 2θ = 0.5° to 130°, with increment D2J: (0.034°), voltage of 40 kV, current of 40 mA, power of 1.6 kW and counting time of 0.5 sec/step. Generated data was analyzed by OriginPro and resultant peaks 2 theta values were compared with the standard Ag NPs

values from the International Center for Diffraction Data (ICDD) database. The average crystal particle size was calculated using Debye-Scherrer's formula given as;

$$\phi = \frac{0.9\lambda}{\beta \cos\theta}$$

Where ø is the crystal particle size, β is full width at half maximum (FWHM), λ is the X-ray wavelength, is angle subtended in peak

Fourier transform infrared spectroscopy (FTIR)

Fourier transform Infrared spectroscopy with a PerkinElmer Spectrum RX I Fourier transform IR system with a frequency ranging from 400 to 4000 cm^{-1} and a resolution of $4cm^{-1}$, set to perform at least 64 scans per sample was used to investigate the organic functional groups of the plant extracts used in the bio-reduction of silver nitrate to silver nanoparticles as follows; 2 mg of silver nanoparticles and 2 g of Potassium bromide (KBr) were desiccated at 200°C under reduced pressure over night. The dried silver nanoparticles were standardized with 100 mg of KBr and then hard pressed to form very thin transparent circular pellets. The pallets were screened at 4000–400 cm^{-1} Wavenumber range. A KBr pellet was used as to plot the baseline.

Dynamic light scattering (DLS) and zeta potential

Zeta sizer Nano ZS Malvern Panalytical was used to evaluate the size distribution and zeta potential of silver nanoparticles. The Zeta sizer Nano ZS instrument was set to perform 60 scan times three times per sample to obtain mean size distribution of nanoparticles. The DLS technique was employed to analyze the nanoparticle size distribution according to standard method with some modifications (Chattopadhyay et al., 2013a). The concentration of silver nanoparticles of 100 µg/mL was sonicated for 5 minutes to disaggregate the nanoparticles, and dynamic particle sizes were determined by suspending 0.5 µl of the sonicated nanoparticle suspension in 1ml of Millipore water in zetasizer cuvette followed by scanning of the nanoparticle suspension by a DLS analyzer. The zeta potential of silver nanoparticles was measured by Zetasizer-Nano ZS using the electrophoretic light scattering technology where 1 mg/mL of nanoparticle suspension was prepared in Milli-Q water in a 900 µl zeta sizer disposable cell. The suspension was screened 60 times per scan for three scans to compute the mean zeta potential of silver nanoparticles.

Scanning electron microscopy (SEM)

The size and morphology of the biosynthesized AgNPs were examined by Field Emission Scanning Electron Microscopy (FESEM), Carl Zeiss SIGMA model operated at 5 kV. Briefly, a thin film of AgNPs was prepared by spreading 1 mg of each sample on carbon tape followed by coating with carbon. Surface images were captured at different magnifications. ImageJ software was used to estimate the size distribution of AgNPs.

Silver Nanoparticles susceptibility bioassay:

Antibacterial activity was assessed by agar well diffusion method.

Carbapenem resistant *E. coli* ATCC 96522 and *K. pneumoniae* NTCT 9633 obtained from the archives of Microbiology department CHS, Makerere University were resuscitated in Tryptone soy broth (TSB) and incubated anaerobically at 37°C for 24 hours, then sub cultured on MacConkey agar plates anaerobically at 37°C for overnight. The fresh all night grown cultures were used to prepare a McFarland's turbidity standard equivalent to 0.5 McFarland's units. *E. coli* and *K. pneumoniae* lawns were inoculated on two separate sterile Muller Hinton Agar plates with a sterile spreader according to manufacturer Oxoid UK using the adjusted McFarland's turbidity standard. Three wells labeled positive control (+ve), negative control (-ve), and Ag NP were bore into the agar plates containing the bacterial lawns using sterile cork borer. Using a dilution factor of 1:2, Ag NPs were diluted using DMSO in bejou bottles and mixed thoroughly and 50µl of the resultant diluent was pipetted into the well labelled Ag NPs. Iminepem disk was used as a positive control while distilled water in DMSO was used as a negative control. The setup was left to set for a minimum of 30 minutes and then incubated at 37°C for 24 hours anaerobically and then checked for antibacterial activity. The zone of clearance for positive control (+ve), negative control (-ve), AgNPs were measured and recorded in millimeters. The experiment was replicated thrice to get the average inhibitory zone.

Determination of Minimum Inhibitory Concentration (MIC) of photosynthesized AgNPs

To assess the MIC, 0.1 g of AgNPs was dissolved in 0.6ml of sterile distilled de-ionized water in a sterile Eppendorf tube and mixed thoroughly by vortexing to form a solution. Then a setup of 8 wells of each extract on the micro titer plate was filled with 0.05ml of sterile TSB. Two-fold serial dilution was carried out on by transfer of 0.05ml of the Ag NP solution from the first well to the eighth well on the micro titer plate containing 0.05ml of sterile Tryptic soy Broth (prepared according to manufacturer Oxoid UK). 0.5µl of 0.5McFarland's turbidity standard prepared by suspension of fresh bacterial culture of *E. coli* and *K. pneumoniae* in separate test tubes, were dispensed into their corresponding wells containing diluted Ag NPs and incubated aerobically at 37°C for an overnight followed by plating of samples from each well on MHA and left to all night at 37^{o}C under aerobic conditions. MIC was determined from the dilution factor with minimum growth inhibition.

Determination of Minimum Bactericidal Concentration (MBC) of biosynthesized AgNPS

Minimum bactericidal concentration was determined by further performing a tenfold serial dilution (1/10 and 1/100) for the dilutions that didn't show growth under MIC determinations on the MHA plate. The two dilutions were further plated on MHA plates that were incubated at 37°C. After incubation the plates were observed for growth, MBC was determined from the dilution next to one which has growth.

Data analysis

Data analysis was done using Origin version 2019b. Comparison of mean zone (diameter in millimeter) of inhibition for CSE-AgNPs and PAE-AgNPs was computed by one-way ANOVA. A P-value of ≤ 0.05 indicated substantial statistical variance.

Results

Characterization of green synthesized silver nanoparticles

UV-Vis spectroscopy

UV-Vis absorbance spectra of PAE and CSE loaded silver nanoparticles solutions were recorded at different time intervals of 0, 0.5, 1, 2, 3, 4, 6, 8, 10, 12, 24 and 72 hours, 0, 0.5, 1, 2, 3, 4 and 5 hours for PAE and CSE respectively. The typical surface plasmon resonance (SPR) peaks for PAE and CSE generated silver nanoparticles were obtained between 417 nm to 475 nm and 430 nm to 456nm respectively. On the other hand, no SPR peaks were registered for the plant extracts alone throughout the experiment duration; at 0 minutes, 0.5, 1, 2 and 3 hours for all PAE-$AgNO_3$ treatments; at 0 minutes for 2%, 4%, 8% and 16% CSE. Increase in the plant extracts concentration resulted into gradual broadening and shifting of the SPR peaks towards the long wavelength; there was a shift of SPR peaks from 434 nm for 2% PAE to 472 nm for 8% PAE. Likewise, a shift from 430 nm for 2% to 461 nm for 8% and 16% CSE was registered, but more prominent in PAE photosynthesized nanoparticles. Identical UV Vis absorbance spectra were observed for 8% and 16% CSE synthesized nanoparticles, Tables S1 and S2; Figs 1-3. Furthermore, it's worth noting that the SPR for AgNPs was attained after 30 minutes with a high absorbance of 3.10 arb. units for CSE and at 4 hours, 6 hours and 8 hours with very low absorbance for 4%, 8%, and 2% ;16% PAE respectively. However, 16% PAE had the highest absorbance of 2.40 at 12 hours, Tables S1 and S2. Furthermore, SPR bands between 260 nm and 300 nm where registered, Figs 2 and 3. PAE and CSE mediated photosynthesis of AgNPs was additionally confirmed by transition from light brown to deep brown colour for PAE and dark blue colour for CSE while Silver nitrate solution and plant extracts remained colourless and light brown respectively throughout the experiment, Fig 4.

X-Ray Diffraction analysis

X-Ray Diffraction analysis generated nine peaks for both PAE and CSE biosynthesized AgNPs positioned at 2θ angles of 27.9˚, 32.2˚, 38.2˚, 44.4˚, 46.3˚, 54.8˚, 57.6˚, 64.5˚, and 77.4˚. However, 38.2˚, 44.4˚, 64.5˚, and 77.4˚ corresponded to crystal planes (111), (200), (220) and (311) respectively. Peak intensity ranged from 1004 to 2824 arb. units and 313 to1174 arb. units for CSE and PAE mediated synthesized Ag NPs. From XRD patterns, the average crystallite size of the silver nanoparticles was computed using the Debye-Scherrer formula. The average crystallite size of PAE and CSE green synthesized silver nanoparticles ranged from 9 to 32 nm (mean = 17 nm) and 13 to 29 nm (mean = 21 nm) respectively, Table 2; Fig 5.

Table 2: 2θ values with their corresponding miller's incidences, peak intensity and average crystal size of CSE and PAE biologically synthesized nanoparticles

2θ (Degree)	Crystal plane	Ag^0-CSE Intensity (arb. Unit)	FWHM (Rad)	Average crystal particle size (nm)	Ag^0-PAE Intensity (arb. units)	FWHM (Rad)	Average crystal particle size (nm)
38.2	(111)	2824	0.01212	13	1174	0.02004	9
44.4	(200)	1004	0.01212	13	312	0.02004	10
64.5	(220)	1077	0.01212	29	409	0.02004	16
77.4	(311)	1159	0.01212	27	435	0.02004	32
Mean				**21**			**17**

Fourier Transform Infra-red Spectrometry Analysis

FTIR spectra of PAE and CSE exhibited similar bands within wavenumber ranges (cm^{-1}) of 3650-3400, 2960-2850, 2349, 2140-1990, 1650-1550, 1370-1390 and 800-400. Furthermore, Ag NPs biosynthesized by CSE were also capped by unique functional groups with spectra wavenumber ranges (cm^{-1}) of 1390-1370 and 1250-1020 while PAE green synthesized Ag NPs exhibited distinctive organic functional groups within wavenumber series (cm^{-1}) of 4000-3700, 1560-1500, 1440-1395, 1310-1250 and 1124-1087, Table 3; Fig 6.

Table 3: AgNPs-CSE and AgNPs-PAE associated organic functional groups as revealed by FTIR analysis

Peak intensity	CSE-Ag NPs Wavenumber (cm^{-1})	PAE-Ag NPs Wavenumber (cm^{-1})	Functional group wavenumber range (cm^{-1})	Bond	Functional group
Low	-	3846.8	3700-4000	O-H	Water
Low	-	3743.4	3700-4000	O-H	Water
High	3428.9	3402.5	3400-3650	O-H	Alcohol or phenols
low	2925.2	-	2960-2850	C-H	Alkane
Low	2360.0	2360.0	2349	O=C=O	Carbon dioxide
Low	2065.5	2065.5	2140-1990	N=C=S	isothiocyanate
Medium	1629.8	1612.2	1650-1550	N-H	Primary amine
Low	-	1517.6	1560-1500	N-H	Secondary amide
Low	-	1438.0	1440-1395	O-H	Carboxylic acid
Low	1376.8	1376.8	1370-1390	C-H	Alkanes
Low	-	1282.3	1310-1250	C-O	Aromatic ester
Low	1211.9	-	1250-1020	C-N	Amines
Medium	1090.9	-	1250-1020	C-N	Amines
medium	-	1108.5	1124-1087	C-O	Secondary alcohol
Medium	613.6	604.8	600-800	C-Cl	Alkyl halide

Silver nanoparticles size distribution and zeta potential

Dynamic light scattering revealed that the size distribution of silver nanoparticles biosynthesized by CSE ranged from 1 nm to 191 nm with mean diameter of 51 nm and mean zeta potential of +0.9 mV. For PAE green synthesized nanoparticles, size distribution ranged from 1nm to 220 nm with average diameter of 59 nm and mean zeta potential of +6.3 mV

Surface morphology analysis

Surface morphology analysis by FESEM shows that PAE and CSE biosynthesized AgNPs were mainly spherical in shape and aggregated in layers, Fig, 7. As the concentration of the plant extracts used increased from 2% to 16%, the level of aggregation increased to form large clusters with slimy material on the surface and between individual nanoparticles and aggregates and is more evident for PAE photosynthesized nanoparticles. Nanoparticle size computation by ImagaJ software from FESEM images showed that the nanoparticles size distribution ranged from approximately 3 nm to 98 nm and 4 nm to 94 nm for CSE and PAE biosynthesized AgNPs respectively. The average size distribution of nanoparticles decreased from 10 nm to 16 nm and 13 nm to 19 nm for CSE-AgNPs and PAE-AgNPs respectively as the concentration of plant extracts increased from 2% to 16%.

AgNPs susceptibility assay

PAE and CSE green synthesized AgNPs demonstrated potent antibacterial activity with statistically similar growth suppression zones of up to 21 mm for carbapenem resistant (CR) and sensitive E. coli and K. pneumoniae. Furthermore, low MICs and MBCs were registered for the biosynthesized AgNPs, Tables 4-5.

Table 4: MIC and MBC values of AgNPs against Carbapenem resistant E. coli and K. pneumoniae.

Bacteria type	MIC (m*g/ml*)	MBC (m*g/ml*)		
	PAE-AgNPs	CSE-AgNPs	PAE-AgNPs	CSE-AgNPs
Carbapenem resistant *E. coli*	0.125	0.125	0.25	0.25
Carbapenem resistant *K. pneumoniae*	0.25	0.25	0.5	0.5

MIC: Minimum inhibitory concentration, MBC: Minimum bactericidal concentration, PAE-AgNPs: *Prunus africana* extract biosynthesized silver nanoparticles and CSE-AgNPs and *Camellia sinensis* extract biosynthesized silver nanoparticles

Table 5: Sensitivity tests of AgNPs green synthesized by PAE and CSE extract showing inhibitory zone in millimeters

Organism	Distilled water Inhibitory zone (mm)	Imipenem disk inhibitory zone (mm)	PAE-Ag NPs inhibitory zone (mm)	CSE-Ag NPs inhibitory zone (mm)
Carbapenem resistant *E. coli*	0^{A}	10^{B}	18^{D}	21^{D}
Carbapenem sensitive *E. coli*	0^{A}	40^{C}	18^{D}	21^{D}
Carbapenem resistant *K. pneumoniae*	0^{A}	8^{B}	20^{D}	20^{D}
Carbapenem sensitive *K. pneumoniae*	0^{A}	40^{C}	20^{D}	19^{D}

Mean values in each column accompanied by the same letter are not significantly different (P > 0.05) (Tukey Multiple Comparison) and values accompanied by letter (s) which are not similar are significantly different (P < 0.05). PAE-AgNPs: Prunus africana extract biosynthesized silver nanoparticles and CSE-AgNPs: Camellia sinensis extract biosynthesized silver nanoparticles

Discussion

The reduction process of silver ions to Ag NPs was indicated by change in color of the reaction mixture from pale brown to dark brown for PAE and dark blue for CSE which was observed macroscopically. Additionally, Ag NP synthesis was confirmed and monitored with UV Vis Spectrophotometry. UV-Vis spectroscopy is a valuable tool for basic characterization and monitoring of the process of nanoparticle synthesis and stability. This is due to the distinctive optical properties of nanoparticles that enable them to intensely interact with specific wavelengths of UV visible light spectrum (Kelly, Coronado, Zhao, & Schatz, 2003; Lee & El-Sayed, 2006; Sastry, Patil, & Sainkar, 1998). Metal surfaces are comparable to plasma, hence possess free electrons in the conductance region and positively charged nuclei. In Ag NPs, the forbidden gap between conduction and valence bands is very minute which allows free movement of electrons. This free movement of electrons generate a surface plasmon resonance (SPR) absorption band, owing to the mutual oscillation of Ag NPs electrons in resonance with the light wave (Das, Nath, Chakdar, Gope, & Bhattacharjee, 2010; Tomaszewska et al., 2013). In this study, the primary characterization and evaluation of CSE and PAE mediated Ag NPs green synthesis by UV Vis absorbance spectral was successful. UV Vis spectroscopy registered sharp absorbance SPR band at wavelengths ranging from 436 nm to 475nm for PAE and 430 nm to 456 nm for CSE which is a unique optical property for Ag NPs (Njagi et al., 2011). Comparable findings were reported in other phytochemical mediated Ag NPs green synthesis studies (Anandalakshmi, Venugobal, & Ramasamy, 2016; Kagithoju, Godishala, & Nanna, 2015; Mohamed et al., 2019; Sahni, Panwar, & Kaur, 2015; Venugopal et al., 2017). The effect of reaction time and plant extract concentration on green synthesis of nanoparticles was analyzed. The absorption spectra exhibited that the SPR peak rises with increasing extract concentration and time. Therefore, high concentration of PAE and CSE avail time dependent optimum amount of bioactive ingredients required to reduce silver ions to silver nanoparticles. Contrary to this, no SPR peak was observed for the highest concentration (16%) of CSE used in this study. Furthermore, broadening of the SPR peaks and shift from the blue wavelength towards the long wavelength with increasing concentration of the plant extracts was registered. This is attributed to increase in size and change in shape of NPs, decrease in the NPs interspace and agglomeration of NPs in colloidal dielectric solutions (Kelly et al., 2003; Lee & El-Sayed, 2006). This specifies that highly concentrated plant extracts mostly PAE synthesizes clustered and polydispersed nanoparticles. SPR peaks were registered between 260 nm and 300 nm not within the optical range of silver nanoparticles. Shaik et al., (Shaik et al., 2018) reported similar findings and attributed the SPR bands to absorbance by compounds with benzene and aromatic rings. These bands are associated with $\pi \rightarrow \pi^*$ transition (Nasrollahzadeh, Sajadi, Babaei, & Maham, 2015; Nasrollahzadeh, Sajadi, & Khalaj, 2014) and validate the binding of polyphenolics and antioxidant-like compounds with aromatic rings in the plant extracts to the surface of silver nanoparticles (Shaik et al., 2018).

XRD analysis agreed with UV Vis spectroscopy results. Peaks of Ag NPs were displayed in the XRD OriginPro plots ratifying presence of Ag NPs. XRD array showed four strong peaks located at 2θ values of 38.0˚, 44.3˚, 64.5˚, and 77.4˚. It's worth noting that these values are identical for both PAE and CSE green synthesized NPs. These values harmonized well with the cubic crystal lattice planes, (111), (200), (220) and (311) respectively of silver metal using International Centre for Diffraction Data (ICDD) database PDF file number 004-0783. However, AgNPs biosynthesized by CSE were of high crystallinity in nature as demonstrated by peaks of higher intensity. Other peaks are corresponding to impurities such as phytochemicals used in the bio-fabrication of AgNPs.

FTIR spectroscopy was employed to profile the phytochemicals in PAE and CSE used in bio-reduction of silver ions to nano-scale by identification of the possible organic functional groups capping the Ag NPs (http://www.ifsc.usp.br/~lavfis2/BancoApostilasImagens/ApLuminescencia/IR_spectroscopy_LM.pdf, accessed on 28/11/2019; https://chem.libretexts.org/Bookshelves/Organic_Chemistry/Map%3A_Organic_Chemistry(Wade)/11%3A_Infrared_Spectroscopy_and_Mass_Spectrometry/11. accessed on 28/11/2019; https://www.sigmaaldrich.com/technical-documents/articles/biology/ir-spectrum-table.html, accessed on 28/11/2019; https://www.thermofisher.com/blog/materials/a-gift-for-you-an-ftir-basic-organic-functional-group-reference-chart/; Pongpiacha, 2014; Silverstein, Bassler, & Morril, 1962). FTIR spectra of PAE and CSE exhibited similar bands within wavenumber ranges (cm^{-1}) of 3650 – 3400, 2960 – 2850, 2349, 2140 – 1990, 1650 – 1550, 1390 – 1370 and 600–800 assigned to O-H intermolecular stretching bonds found in alcohol or phenols, C-H stretching vibrations in methyl groups alkanes, O = C = O stretching bonds of carbon dioxide, N = C = S stretching bonds of isothiocyanate, N-H bending oscillations of primary amines, C-H bending bonds of gem dimethyl groups in alkanes and C-Cl stretching bond of halide alkyl correspondingly. However, Ag NPs biosynthesized by CSE were also capped by unique functional groups with spectra wavenumber ranges (cm^{-1}) of 1390 – 1370 and 1250 – 1020 associated stretching vibrations of O-H group in alcohols or phenols and C-N of amine respectively. Additionally, PAE green synthesized Ag NPs exhibited distinctive organic functional groups within wavenumber series (cm^{-1}) of 4000 – 3700, 1560 – 1500, 1440 – 1395, 1310 – 1250 and 1124 – 1087 associated with free OH probably due to water, N-H stretching vibrations due secondary amine, O-H bending vibrations in carboxylic acid group and C-O stretching vibrations of secondary alcohol respectively.

Similar to these findings, green tea polyphenols catechins exhibited OH intermolecular bonds linked to methyl functional groups of the different constituent units (Botten, Fugallo, Fraternali, & Molteni, 2015).

Owing to its undisputed efficacy in sub-Saharan Africa, PAE has been patented in France as an anti-prostate cancer and benign prostate hyperplasia (BPH) agent (Schleich, Papaioannou, Baniahmad, & Matusch, 2006). The confirmed phytochemicals in PAE are; pentacyclic triterpenoids (ursolic and oleanolic acids) which possess terminal OH and COOH groups (Donovan et al., 1998), phytosterols chiefly β-sitosterol and β-sitostenone with OH, ethyl and methyl as the main functional groups (Bin Sayeed, Karim, Sharmin, & Morshed, 2016; Carbin, Larsson, & Lindahl, 1990), Ferulic acid esters (n-tetracosanol and n-docosanol) having COOH, -CHO, -CH2OH, -CH3, and -COOC2H5 as their terminal groups and aromatic rings (Kampa et al., 2004; Nenadis, Zhang, & Tsimidou, 2003). This is in agreement with the findings of this study as all these functional groups were registered by FTIR. The three classes of phytochemicals possess synergistic effects which thwart biochemical and morphological alterations associated with Prostate cancer and BPH. Moreover, these phytochemicals possess potent antioxidant activity (Bin Sayeed et al., 2016; Ghante & Jamkhande, 2019; Kikuzaki, Hisamoto, Hirose, Akiyama, & Taniguchi, 2002; Nenadis et al., 2003; Yoshida & Niki, 2003). *Camellia sinesis* processed into green tea contains polyphenols catechins containing OH groups and methyl groups on benzene rings (Botten et al., 2015; T. Takahashi, S. Nagatoishi, D. Kuroda, & K. J. P. o. Tsumoto, 2018). They are subdivided into (−)-epigallocatechin-3-gallate (EGCG), (−)-epigallocatechin, (−)-epicatechin-3-gallate and (−)-epicatechin (EC). Formidable antioxidant activity of catechins most importantly EGCG that affords them to scavenge free radical hence counteracting oxidative stress has been documented (Botten et al., 2015; Forester & Lambert, 2011; Pasrija & Anandharamakrishnan, 2015; RAMÍREZ-ARISTIZABAL, Ortíz, RESTREPO-ARISTIZABAL, & SALINAS-VILLADA, 2017; T. Takahashi, S. Nagatoishi, D. Kuroda, & K. Tsumoto, 2018). Due to its health benefits, green tea is a beverage to 66% of the world's population (Hajiaghaalipour, Sanusi, & Kanthimathi, 2016). This is supported by UV Vis spectroscopy results from this study. CSE synthesized nanoparticles rapidly and at high intensity as compared to PAE.

FESEM images exhibited that AgNPs green synthesized by different concentration of CSE and PAE were spherical in shape. This is in line with other studies which fabricated AgNPs using plant extracts (Ajitha, Ashok Kumar Reddy, & Sreedhara Reddy, 2015; Gholami, Shahzamani, Marzban, & Lashgarian, 2018; Hamouda, Hussein, Abo-Elmagd, & Bawazir, 2019). The nanoparticles were highly aggregated with average size distribution varying from approximately 3 nm to 19 nm for nanoparticles. Clustering of nanoparticles may be attributed to interaction of concentrated nanoparticles with the organic components of the plant extracts used in biosynthesis. This is supported by appearance of a slimy like substance on the surface and in between nanoparticles especially at high concentrations of plant extracts in FESEM images. The procedure used in the preparation of the film of nanoparticles for FESEM imaging also influences the level nanoparticle agglomeration. To characterize the particle size and nanostructure using high resolution scanning electron microscopy (SEM), Chattopadhyay et al., 2013a) recommended a method that prepares films with disaggregated nanoparticles. The improved method involves suspension of nanoparticles in de-ionized water at a concentration of 1 mg/mL followed sonication to form a homogenous suspension. The homogenous suspension is diluted using a 1–20 dilution factor and then 1 µl of the diluent be is spread on to a carbon tape, dried, gold/carbon coated, and images taken.

Antimicrobial activity of nanoparticles depends on size and shape distribution. Nanoscale materials with minute size possess enhanced chemical reactivity, high diffusion rate and high penetrative power while those with various form distribution offer different modes of antimicrobial activity (Ssekatawa et al, 2020; Simon-Deckers et al. 2009). PAE and CSE mediated biosynthesis attained very small nanoparticles as revealed by FESEM, XRD and DLS analyses. However, only the spherical form was achieved by this study. Zeta potential estimation using the DLS technique revealed that PAE and CSE green synthesized AgNPs were positively charged. This promotes electrostatic interface with the negatively charged bacterial cell walls (Dickson and Koohmaraie 1989). Thus, minute and positively charged nanoparticles possess enhanced antibacterial activity (Lu et al., 2013).

The antibacterial potential of the green synthesized AgNPs on human pathogenic CR E. coli and K. pneumoniae was assessed using the growth inhibitory zone. The NPs demonstrated efficient antibacterial activity with the growth inhibitory zones larger than those achieved in other studies (Raman, Park, Sakthivel, & Suresh, 2017). Furthermore, several antimicrobial bactericide efficacies are dose dependent (McKenzie, 2011). However, high concentrations exhibit nonselective cytotoxicity. Therefore, therapeutic agents with very low MIC and MBC are preferable. This study achieved significantly low MIC and MBC of 125/250 µg/ml and 250/500 µg/ml respectively comparable to the recommended NP nontoxic dose (100 µg/mg) to mammalian cells and way below MICs reported by other studies (Jafari et al., 2018; Reithofer, Lakshmanan, Ping, Chin, & Hauser, 2014). The susceptibility pattern of both CR and sensitive *E. coli* and *K. pneumoniae* to AgNPs (MIC = 125 µg/ml for *E. coli* and 250 µg/ml for *K. pneumoniae*) was identical which is an indication of no mechanism of resistance to AgNPs in carbapenemase producing bacteria. Furthermore, compared to CSE-AgNPs, statistically PAE-AgNPs exhibited smaller zones of bacterial growth inhibition. This may be attributed to higher levels of the slimy PAE materials (proteins and polysaccharides) as revealed by FESEM images that might prevent high rate migration of the nanoparticles within the agar.

Conclusion

Evolution of MDR pathogens presents a challenge to health care systems and calls for speedy research to design alternative therapeutics such as NPs without compromising the safety of consumers. Therefore, this study employed an ecofriendly method the green synthesis to yield AgNPs. The *Camellia sinensis* and *Prunus africana* photosynthesized Ag NPs exhibited potent antibacterial activity against CR clinical isolates

Declarations

Ethics and consent to participate: Not applicable

Consent for publication: Not applicable

Funding:

The authors declare that this research project was funded by Africa Centre of Excellence in Materials, Product Development & Nanotechnology; MAPRONANO ACE, Grant No. P151847IDA credit 5797-UG, College of Engineering Design Art and Technology, Makerere University.

Availability of Data and Materials:

All relevant data has been submitted with the manuscript and therefore no supplementary data

Competing interests

The authors declare that they have no competing interests

Authors' contributions

This work was carried out in collaboration between all authors. John Baptist Kirabira (JBK), Malik Maaza (MM) Jesca L. Nakavuma (JLN), Denis K. Byarugaba (DKB), and Francis Ejobi (FB) conceptualized this project. Kenneth Ssekatawa (KS), Eddie Wampande (EW), Charles Kato Drago (CKD) & Juliet Sackey (JS) performed all the laboratory experiments. KS, JBK, JS and MM analyzed the Data, KS, EW, JS and CKD wrote the first draft of the manuscript and managed manuscript revisions. All authors read and approved the final manuscript.

Acknowledgements: We are greatful to MAPRONANO ACE for funding this work, Materials Research Department, iThemba LABS and Chemical Engineering Laboratories, College of Science, Engineering and Technology University of South Africa-Science Campus, Florida for availing laboratory space and materials characterization facilities.

References

Agnihotri, S., Mukherji, S., & Mukherji, S. J. N. (2013). Immobilized silver nanoparticles enhance contact killing and show highest efficacy: elucidation of the mechanism of bactericidal action of silver. *5*(16), 7328-7340.

Ajitha, B., Ashok Kumar Reddy, Y., & Sreedhara Reddy, P. (2015). Green synthesis and characterization of silver nanoparticles using Lantana camara leaf extract. *Mater Sci Eng C Mater Biol Appl, 49*, 373-381. doi:10.1016/j.msec.2015.01.035

Albrecht, M. A., Evans, C. W., & Raston, C. L. J. G. c. (2006). Green chemistry and the health implications of nanoparticles. *8*(5), 417-432.

Anandalakshmi, K., Venugobal, J., & Ramasamy, V. J. A. N. (2016). Characterization of silver nanoparticles by green synthesis method using Pedalium murex leaf extract and their antibacterial activity. *6*(3), 399-408.

Bin Sayeed, M. S., Karim, S. M. R., Sharmin, T., & Morshed, M. M. J. M. (2016). Critical analysis on characterization, systemic effect, and therapeutic potential of beta-sitosterol: a plant-derived orphan phytosterol. *3*(4), 29.

Bondarenko, O., Juganson, K., Ivask, A., Kasemets, K., Mortimer, M., & Kahru, A. J. A. o. t. (2013). Toxicity of Ag, CuO and ZnO nanoparticles to selected environmentally relevant test organisms and mammalian cells in vitro: a critical review. *87*(7), 1181-1200.

Botten, D., Fugallo, G., Fraternali, F., & Molteni, C. (2015). Structural Properties of Green Tea Catechins. *The Journal of Physical Chemistry B, 119*(40), 12860-12867. doi:10.1021/acs.jpcb.5b08737

Carbin, B. E., Larsson, B., & Lindahl, O. J. B. j. o. u. (1990). Treatment of benign prostatic hyperplasia with phytosterols. *66*(6), 639-641.

Castro, L., Blázquez, M. L., González, F. G., & Ballester, A. J. R. i. A. S. E. (2014). Mechanism and applications of metal nanoparticles prepared by bio-mediated process. *3*(3), 199-216.

CDC. (2013). Antibiotic resistance threats in the United States.

Das, R., Nath, S. S., Chakdar, D., Gope, G., & Bhattacharjee, R. J. J. o. E. N. (2010). Synthesis of silver nanoparticles and their optical properties. *5*(4), 357-362.

Dickson, D. P. (1999). Nanostructured magnetism in living systems. *J Journal of Magnetism Magnetic Materials, 203*(1-3), 46-49.

Durán, N., Marcato, P. D., Alves, O. L., De Souza, G. I., & Esposito, E. J. J. o. n. (2005). Mechanistic aspects of biosynthesis of silver nanoparticles by several Fusarium oxysporum strains. *3*(1), 8.

Durán, N., Nakazato, G., & Seabra, A. (2016). Antimicrobial activity of biogenic silver nanoparticles, and silver chloride nanoparticles: an overview and comments. *B %J Applied microbiology biotechnology, 100*(15), 6555-6570.

ECDC. (2017). European Centre for Disease Prevention and Control; Antimicrobial resistance surveillance in Europe 2016. Annual Report of the European Antimicrobial Resistance Surveillance Network (EARS-Net). Stockholm: ECDC; 2017.

Forester, S. C., & Lambert, J. D. J. M. n. f. r. (2011). The role of antioxidant versus pro-oxidant effects of green tea polyphenols in cancer prevention. *55*(6), 844-854.

Fox, C. L., & Modak, S. M. J. A. a. c. (1974). Mechanism of silver sulfadiazine action on burn wound infections. *5*(6), 582-588.

Ghante, M. H., & Jamkhande, P. G. J. J. o. p. (2019). Role of Pentacyclic Triterpenoids in Chemoprevention and Anticancer Treatment: An Overview on Targets and Underling Mechanisms. *22*(2), 55.

Gholami, M., Shahzamani, K., Marzban, A., & Lashgarian, H. E. (2018). Evaluation of antimicrobial activity of synthesised silver nanoparticles using Thymus kotschyanus aqueous extract. *IET Nanobiotechnol, 12*(8), 1114-1117. doi:10.1049/iet-nbt.2018.5110

Gong, P., Li, H., He, X., Wang, K., Hu, J., Tan, W., . . . Yang, X. J. N. (2007). Preparation and antibacterial activity of Fe3O4@ Ag nanoparticles. *18*(28), 285604.

Guzmán, M. G., Dille, J., & Godet, S. J. I. J. C. B. E. (2009). Synthesis of silver nanoparticles by chemical reduction method and their antibacterial activity. *2*(3), 104-111.

Hajiaghaalipour, F., Sanusi, J., & Kanthimathi, M. J. J. o. F. S. (2016). Temperature and time of steeping affect the antioxidant properties of white, green, and black tea infusions. *81*(1), H246-H254.

Hamouda, R. A., Hussein, M. H., Abo-Elmagd, R. A., & Bawazir, S. S. (2019). Synthesis and biological characterization of silver nanoparticles derived from the cyanobacterium Oscillatoria limnetica. *Sci Rep, 9*(1), 13071. doi:10.1038/s41598-019-49444-y

http://www.ifsc.usp.br/~lavfis2/BancoApostilasImagens/ApLuminescencia/IR_spectroscopy_LM.pdf. (accessed on 28/11/2019).

https://chem.libretexts.org/Bookshelves/Organic_Chemistry/Map%3A_Organic_Chemistry(Wade)/11%3A_Infrared_Spectroscopy_and_Mass_Spectrometry/11. accessed on 28/11/2019.

https://www.sigmaaldrich.com/technical-documents/articles/biology/ir-spectrum-table.html. (accessed on 28/11/2019).

https://www.thermofisher.com/blog/materials/a-gift-for-you-an-ftir-basic-organic-functional-group-reference-chart/.

Huang, J., Li, Q., Sun, D., Lu, Y., Su, Y., Yang, X., . . . He, N. J. N. (2007). Biosynthesis of silver and gold nanoparticles by novel sundried Cinnamomum camphora leaf. *18*(10), 105104.

Jafari, A., Jafari Nodooshan, S., Safarkar, R., Movahedzadeh, F., Mosavari, N., Novin Kashani, A., . . . Majidpour, A. (2018). Toxicity effects of AgZnO nanoparticles and rifampicin on Mycobacterium tuberculosis into the macrophage. *58*(1), 41-51. doi:https://doi.org/10.1002/jobm.201700289

Kagithoju, S., Godishala, V., & Nanna, R. S. J. B. (2015). Eco-friendly and green synthesis of silver nanoparticles using leaf extract of Strychnos potatorum Linn. F. and their bactericidal activities. *5*(5), 709-714.

Kampa, M., Alexaki, V.-I., Notas, G., Nifli, A.-P., Nistikaki, A., Hatzoglou, A., . . . Boskou, D. J. B. C. R. (2004). Antiproliferative and apoptotic effects of selective phenolic acids on T47D human breast cancer cells: potential mechanisms of action. *6*(2), R63.

Kawata, K., Osawa, M., & Okabe, S. (2009). In vitro toxicity of silver nanoparticles at noncytotoxic doses to HepG2 human hepatoma cells. *Environ Sci Technol, 43*(15), 6046-6051. doi:10.1021/es900754q

Kayange, N., Kamugisha, E., Mwizamholya, D. L., Jeremiah, S., & Mshana, S. E. J. B. p. (2010). Predictors of positive blood culture and deaths among neonates with suspected neonatal sepsis in a tertiary hospital, Mwanza-Tanzania. *10*(1), 39.

Kelly, K. L., Coronado, E., Zhao, L. L., & Schatz, G. C. (2003). The optical properties of metal nanoparticles: the influence of size, shape, and dielectric environment. In: ACS Publications.

Khan, M., Khan, M., Adil, S. F., Tahir, M. N., Tremel, W., Alkhathlan, H. Z., . . . Siddiqui, M. R. H. J. I. j. o. n. (2013). Green synthesis of silver nanoparticles mediated by Pulicaria glutinosa extract. *8*, 1507.

Kikuzaki, H., Hisamoto, M., Hirose, K., Akiyama, K., & Taniguchi, H. J. J. o. a. f. c. (2002). Antioxidant properties of ferulic acid and its related compounds. *50*(7), 2161-2168.

Kvítek, L., Panáček, A., Soukupova, J., Kolář, M., Večeřová, R., Prucek, R., . . . Zbořil, R. J. T. J. o. P. C. C. (2008). Effect of surfactants and polymers on stability and antibacterial activity of silver nanoparticles (NPs). *112*(15), 5825-5834.

Laxminarayan, R., Boeckel, T. V., & Teillant, A. (2015). The Economic Costs of Withdrawing Antimicrobial Growth Promoters from the Livestock Sector. doi:doi:https://doi.org/10.1787/5js64kst5wvl-en

Lee, K.-S., & El-Sayed, M. A. J. T. J. o. P. C. B. (2006). Gold and silver nanoparticles in sensing and imaging: sensitivity of plasmon response to size, shape, and metal composition. *110*(39), 19220-19225.

Li, S., Shen, Y., Xie, A., Yu, X., Qiu, L., Zhang, L., & Zhang, Q. J. G. C. (2007). Green synthesis of silver nanoparticles using Capsicum annuum L. extract. *9*(8), 852-858.

Li, W.-R., Xie, X.-B., Shi, Q.-S., Zeng, H.-Y., You-Sheng, O.-Y., Chen, Y.-B. J. A. m., & biotechnology. (2010). Antibacterial activity and mechanism of silver nanoparticles on Escherichia coli. *85*(4), 1115-1122.

Livermore, D. M., Warner, M., Mushtaq, S., Doumith, M., Zhang, J., & Woodford, N. J. I. j. o. a. a. (2011). What remains against carbapenem-resistant Enterobacteriaceae? Evaluation of chloramphenicol, ciprofloxacin, colistin, fosfomycin, minocycline, nitrofurantoin, temocillin and tigecycline. *37*(5), 415-419.

Marková, Z., Šišková, K., Filip, J., Šafářová, K., Prucek, R., Panáček, A., . . . Zbořil, R. J. G. C. (2012). Chitosan-based synthesis of magnetically-driven nanocomposites with biogenic magnetite core, controlled silver size, and high antimicrobial activity. *14*(9), 2550-2558.

Martinez-Gutierrez, F., Boegli, L., Agostinho, A., Sánchez, E. M., Bach, H., Ruiz, F., & James, G. J. B. (2013). Anti-biofilm activity of silver nanoparticles against different microorganisms. *29*(6), 651-660.

McKenzie, C. (2011). Antibiotic dosing in critical illness. *Journal of Antimicrobial Chemotherapy, 66*(suppl_2), ii25-ii31. doi:10.1093/jac/dkq516 %J Journal of Antimicrobial Chemotherapy

Mie, R., Samsudin, M. W., Din, L. B., Ahmad, A., Ibrahim, N., & Adnan, S. N. A. J. I. J. o. N. (2014). Synthesis of silver nanoparticles with antibacterial activity using the lichen Parmotrema praesorediosum. *9*, 121.

Mohamed, H. E. A., Afridi, S., Khalil, A. T., Zia, D., Iqbal, J., Ullah, I., . . . Maaza, M. J. M. R. E. (2019). Biosynthesis of silver nanoparticles from Hyphaene thebaica fruits and their in vitro pharmacognostic potential. *6*(10), 1050c1059.

Morones, J. R., Elechiguerra, J. L., Camacho, A., Holt, K., Kouri, J. B., Ramírez, J. T., & Yacaman, M. J. (2005). The bactericidal effect of silver nanoparticles. *Nanotechnology, 16*(10), 2346-2353. doi:10.1088/0957-4484/16/10/059

Moyer, C. A., BRENTANO, L., GRAVENS, D. L., MARGRAF, H. W., & MONAFO, W. W. J. A. o. s. (1965). Treatment of large human burns with 0.5% silver nitrate solution. *90*(6), 812-867.

Nasrollahzadeh, M., Sajadi, S. M., Babaei, F., & Maham, M. (2015). Euphorbia helioscopia Linn as a green source for synthesis of silver nanoparticles and their optical and catalytic properties. *%J Journal of colloid interface science, 450*, 374-380.

Nasrollahzadeh, M., Sajadi, S. M., & Khalaj, M. J. R. A. (2014). Green synthesis of copper nanoparticles using aqueous extract of the leaves of Euphorbia esula L and their catalytic activity for ligand-free Ullmann-coupling reaction and reduction of 4-nitrophenol. *4*(88), 47313-47318.

Nenadis, N., Zhang, H. Y., & Tsimidou, M. Z. (2003). Structure-antioxidant activity relationship of ferulic acid derivatives: effect of carbon side chain characteristic groups. *J Agric Food Chem, 51*(7), 1874-1879. doi:10.1021/jf0261452

Njagi, E. C., Huang, H., Stafford, L., Genuino, H., Galindo, H. M., Collins, J. B., . . . Suib, S. L. J. L. (2011). Biosynthesis of iron and silver nanoparticles at room temperature using aqueous sorghum bran extracts. *27*(1), 264-271.

Panáček, A., Kvitek, L., Prucek, R., Kolář, M., Večeřová, R., Pizúrová, N., . . . Zbořil, R. J. T. J. o. P. C. B. (2006). Silver colloid nanoparticles: synthesis, characterization, and their antibacterial activity. *110*(33), 16248-16253.

Pasrija, D., & Anandharamakrishnan, C. J. F. B. T. (2015). Techniques for extraction of green tea polyphenols: a review. *8*(5), 935-950.

Polavarapu, L., & Liz-Marzán, L. M. J. N. (2013). Growth and galvanic replacement of silver nanocubes in organic media. *5*(10), 4355-4361.

Pongpiacha, S. J. J. (2014). FTIR spectra of organic functional group compositions in PM2. 5 collected at Chiang-Mai City, Thailand during the haze episode in March 2012. *14*(22), 2967-2977. doi:DOI: 10.3923/jas.2014.2967.2977

Raman, G., Park, S. J., Sakthivel, N., & Suresh, A. K. (2017). Physico-cultural parameters during AgNPs biotransformation with bactericidal activity against human pathogens. *Enzyme and Microbial Technology, 100*, 45-51. doi:https://doi.org/10.1016/j.enzmictec.2017.02.002

RAMÍREZ-ARISTIZABAL, L. S., Ortíz, A., RESTREPO-ARISTIZABAL, M. F., & SALINAS-VILLADA, J. F. J. V. (2017). Comparative study of the antioxidant capacity in green tea by extraction at different temperatures of four brands sold in Colombia. *24*(2), 132-145.

Reithofer, M. R., Lakshmanan, A., Ping, A. T. K., Chin, J. M., & Hauser, C. A. E. (2014). In situ synthesis of size-controlled, stable silver nanoparticles within ultrashort peptide hydrogels and their anti-bacterial properties. *Biomaterials, 35*(26), 7535-7542. doi:10.1016/j.biomaterials.2014.04.102

Rizzello, L., Cingolani, R., & Pompa, P. P. (2013). Nanotechnology tools for antibacterial materials. *J Nanomedicine, 8*(5), 807-821.

Roca, A., Quintó, L., Abacassamo, F., Morais, L., Vallès, X., Espasa, M., . . . Health, I. (2008). Invasive Haemophilus influenzae disease in children less than 5 years of age in Manhiça, a rural area of southern Mozambique. *13*(6), 818-826.

Sahni, G., Panwar, A., & Kaur, B. J. I. N. L. (2015). Controlled green synthesis of silver nanoparticles by Allium cepa and Musa acuminata with strong antimicrobial activity. *5*(2), 93-100.

Sastry, M., Patil, V., & Sainkar, S. J. t. j. o. p. c. B. (1998). Electrostatically controlled diffusion of carboxylic acid derivatized silver colloidal particles in thermally evaporated fatty amine films. *102*(8), 1404-1410.

Schleich, S., Papaioannou, M., Baniahmad, A., & Matusch, R. J. P. m. (2006). Extracts from Pygeum africanum and other ethnobotanical species with antiandrogenic activity. *72*(09), 807-813.

Shaik, M. R., Khan, M., Kuniyil, M., Al-Warthan, A., Alkhathlan, H. Z., Siddiqui, M. R. H., . . . Khan, M. J. S. (2018). Plant-extract-assisted green synthesis of silver nanoparticles using Origanum vulgare L. extract and their microbicidal activities. *10*(4), 913.

Silverstein, R. M., Bassler, G. C., & Morril, T. (1962). Spectrometric identification of organic compounds. *%J Journal of Chemical Education, 39*(11), 546.

Tahir, M. N., Natalio, F., Cambaz, M. A., Panthöfer, M., Branscheid, R., Kolb, U., & Tremel, W. (2013). Controlled synthesis of linear and branched Au@ZnO hybrid nanocrystals and their photocatalytic properties. *Nanoscale, 5*(20), 9944-9949. doi:10.1039/C3NR02817H

Takahashi, T., Nagatoishi, S., Kuroda, D., & Tsumoto, K. (2018). Thermodynamic and computational analyses reveal the functional roles of the galloyl group of tea catechins in molecular recognition. *PLOS ONE, 13*(10), e0204856. doi:10.1371/journal.pone.0204856

Takahashi, T., Nagatoishi, S., Kuroda, D., & Tsumoto, K. J. P. o. (2018). Thermodynamic and computational analyses reveal the functional roles of the galloyl group of tea catechins in molecular recognition. *13*(10), e0204856.

Tomaszewska, E., Soliwoda, K., Kadziola, K., Tkacz-Szczesna, B., Celichowski, G., Cichomski, M., . . . Grobelny, J. J. J. o. N. (2013). Detection limits of DLS and UV-Vis spectroscopy in characterization of polydisperse nanoparticles colloids. *2013*.

Venugopal, K., Rather, H., Rajagopal, K., Shanthi, M., Sheriff, K., Illiyas, M., . . . Biology, P. B. (2017). Synthesis of silver nanoparticles (Ag NPs) for anticancer activities (MCF 7 breast and A549 lung cell lines) of the crude extract of Syzygium aromaticum. *167*, 282-289.

Wang, L., Hu, C., & Shao, L. J. I. j. o. n. (2017). The antimicrobial activity of nanoparticles: present situation and prospects for the future. *12*, 1227.

Yin, I. X., Zhang, J., Zhao, I. S., Mei, M. L., Li, Q., & Chu, C. H. J. I. J. o. N. (2020). The Antibacterial Mechanism of Silver Nanoparticles and Its Application in Dentistry. *15*, 2555.

Yoshida, Y., & Niki, E. (2003). Antioxidant effects of phytosterol and its components. J Nutr Sci Vitaminol (Tokyo). *%J Chemistry physics of lipids*

123(1), 63-75.

Simon-Deckers A, Loo S, Mayne-L'hermite M, Herlin-Boime N, Menguy N, Reynaud C et al (2009) Size-, composition- and shape-dependent toxicological of metal oxide nanoparticles and carbon nanotubes toward bacteria. Environ Sci Technol43:8423–8429

Ssekatawa, K., Byarugaba, D.K., Kato, C.D., Ejobi F., Tweyongyere R., Lubwama M., Kirabira JB & Wampande EM. Nanotechnological solutions for controlling transmission and emergence of antimicrobial-resistant bacteria, future prospects, and challenges: a systematic review. J Nanopart Res 22, 117 (2020). https://doi.org/10.1007/s11051-020-04817-7

Lu Z, Rong K, Li J, Yang H, Chen R. (2013). Size-dependent antibacterial activities of silver nanoparticles against oral anaerobic pathogenic bacteria. J Mater Sci Mater Med 24:1465–1471

Dickson JS and Koohmaraie M. (1989). Cell Surface Charge Characteristics and Their Relationship to Bacterial Attachment to Meat Surfaces. APPLIED AND ENVIRONMENTAL MICROBIOLOGY, Apr. 1989, p. 832-836

Figures

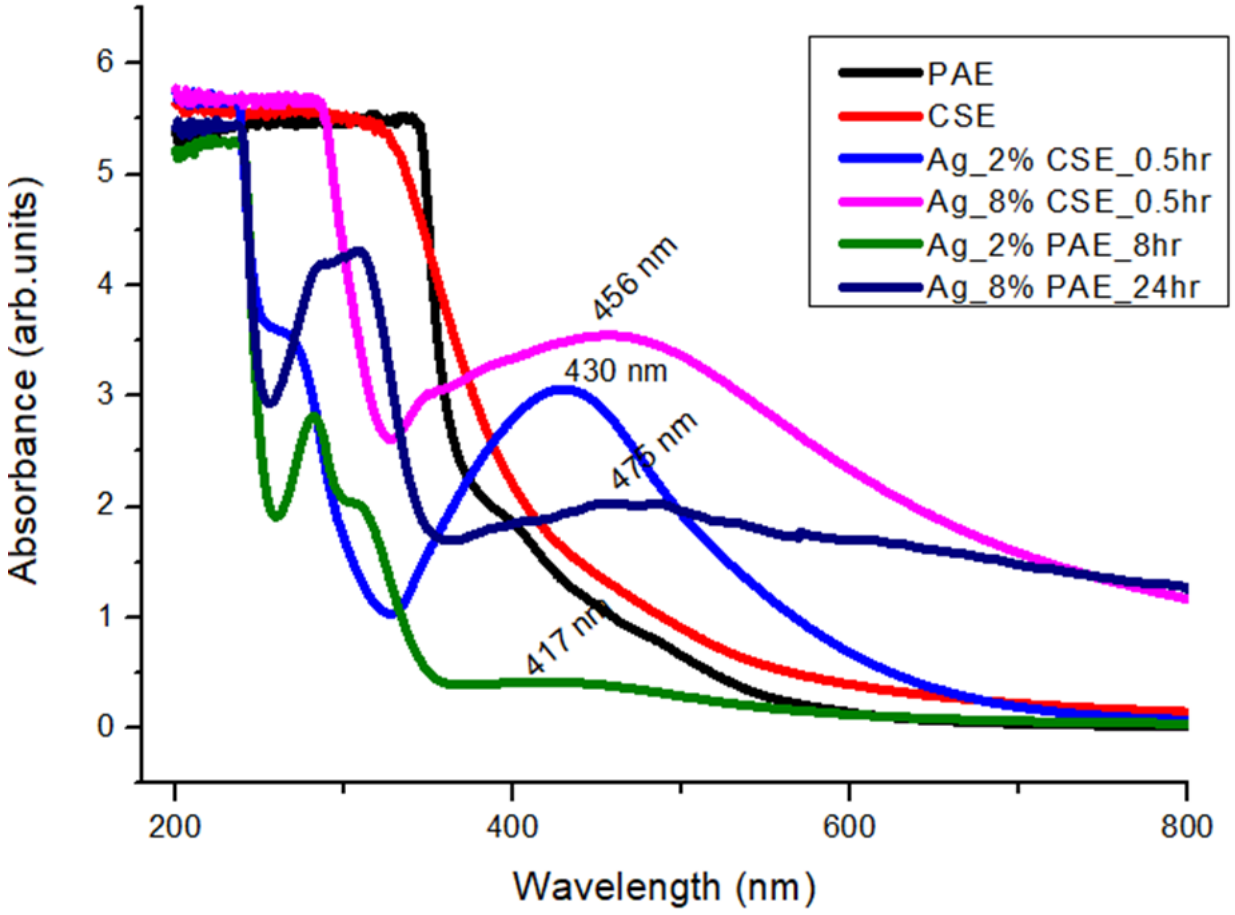

Figure 1

UV Vis absorbance spectra comparing the rate green synthesis of Age Ps by different concentrations of C SE and PAE

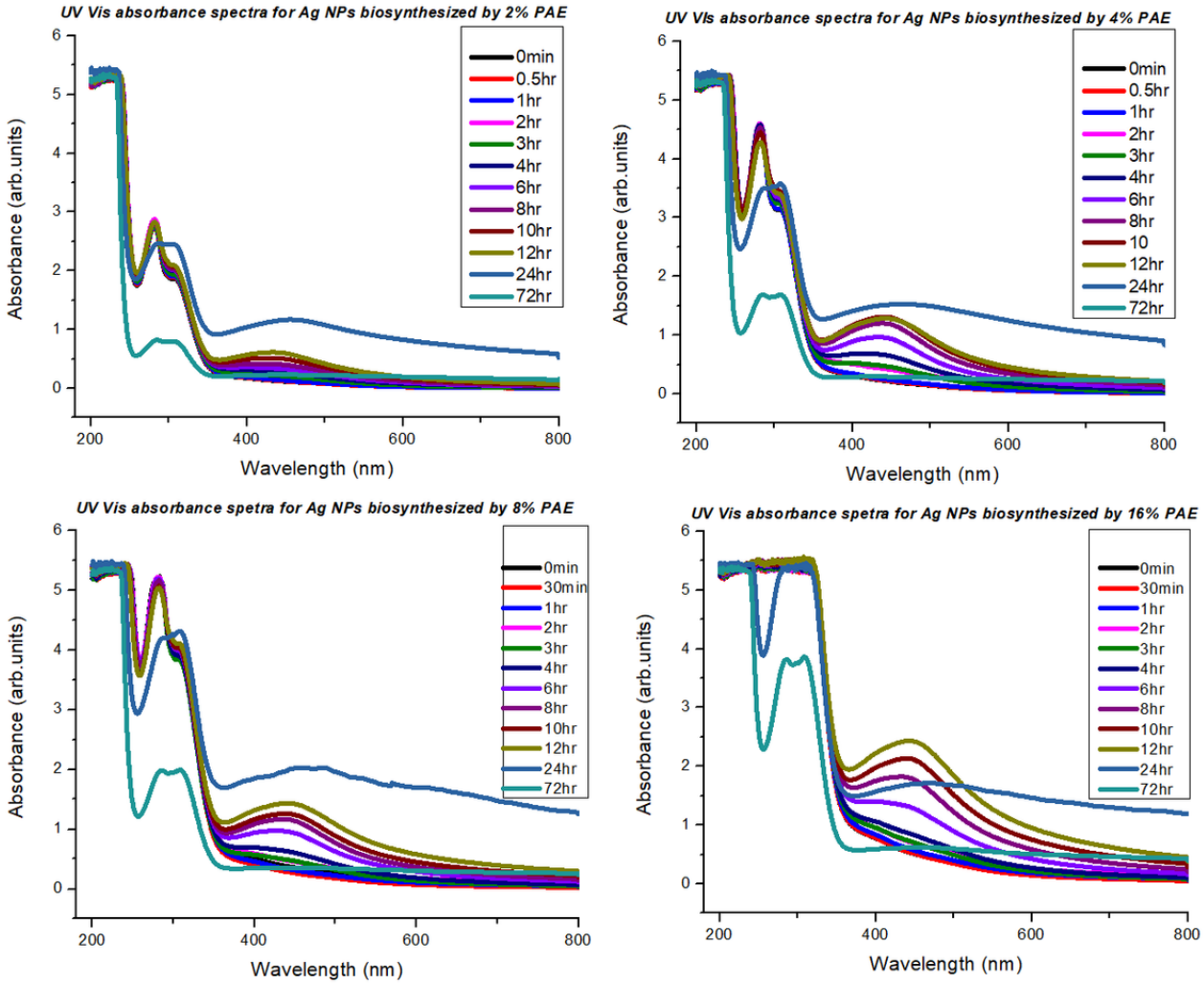

Figure 2

UV Vis absorbance spectra monitoring silver nanoparticle PAE mediated biosynthesis and stability

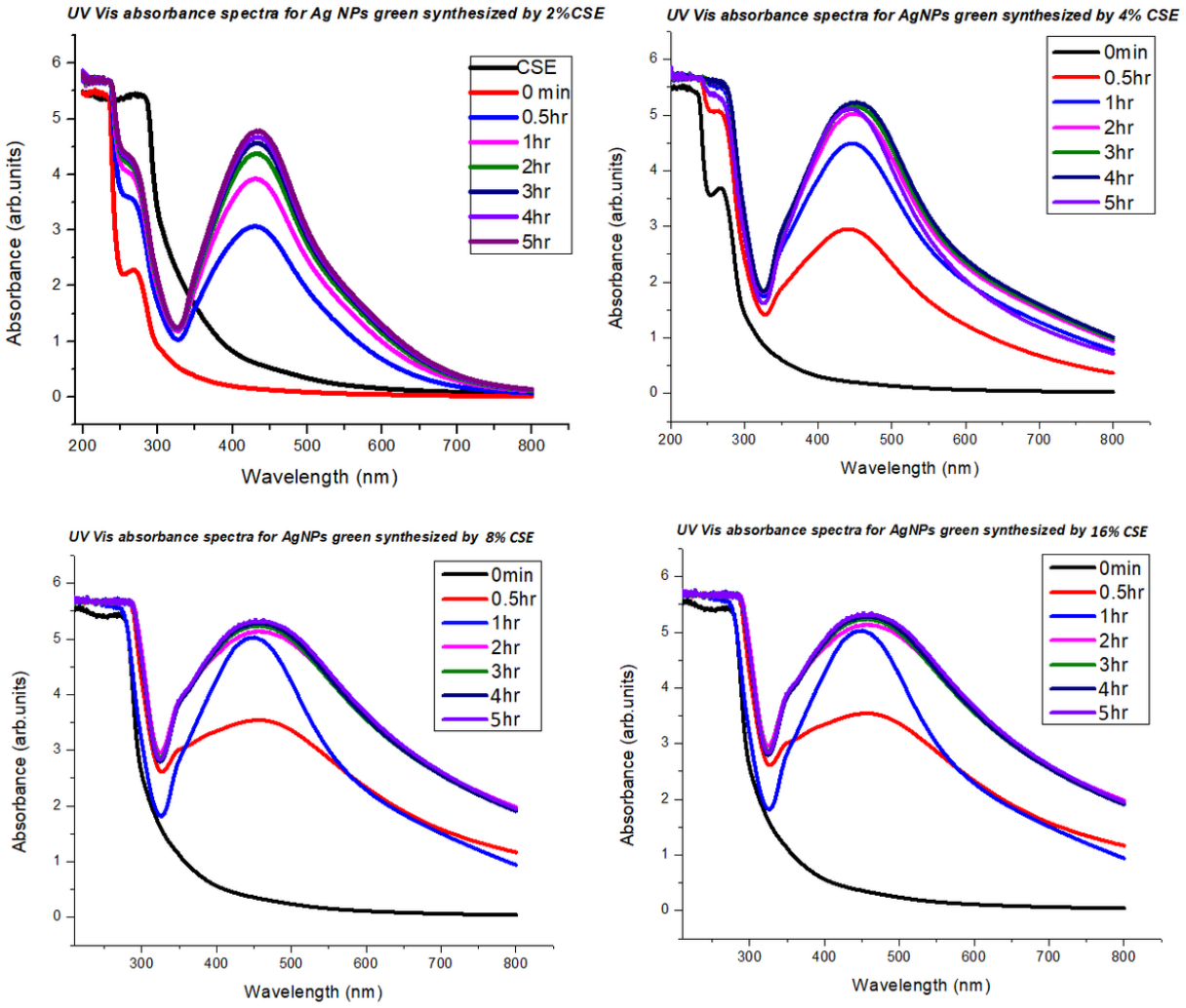

Figure 3

UV Vis absorbance spectra monitoring silver nanoparticle CSE mediated biosynthesis and stability

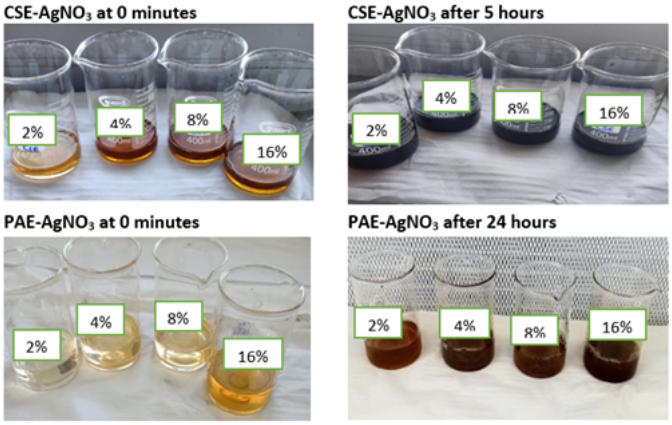

Figure 4

Colour transition from light brown at 0 minutes to dark blue for CSE- AgNO3 and dark brown for PAE-AgNO3 suspension

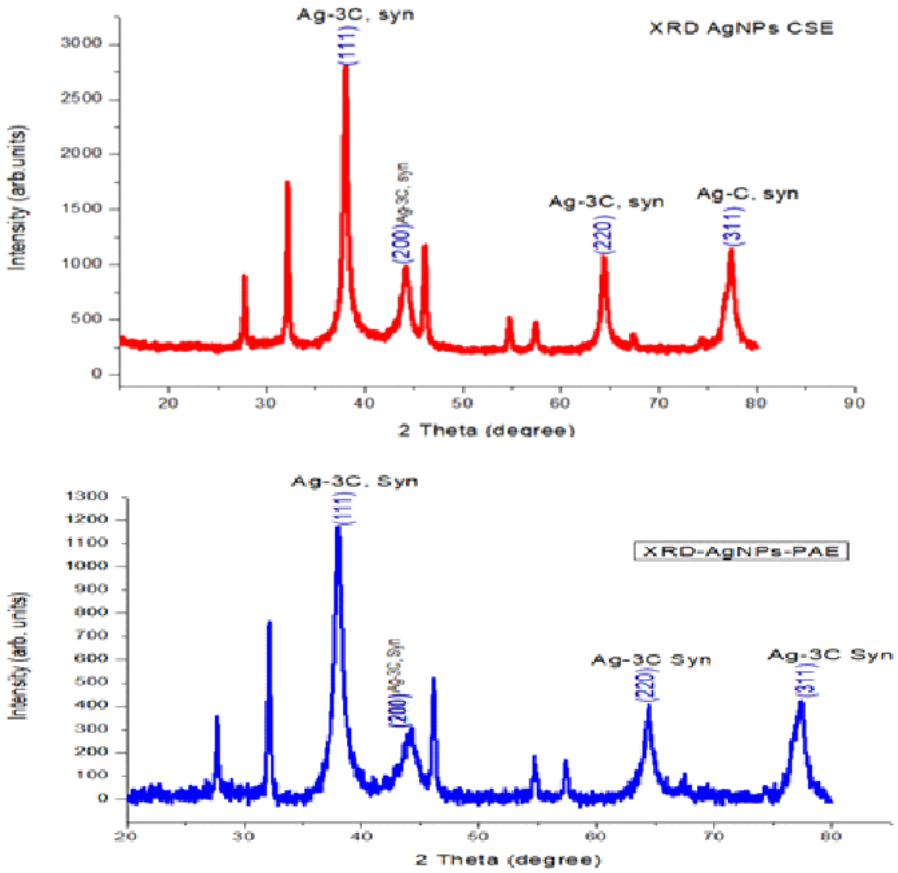

Figure 5

XRD pattern for green synthesized AgNPs

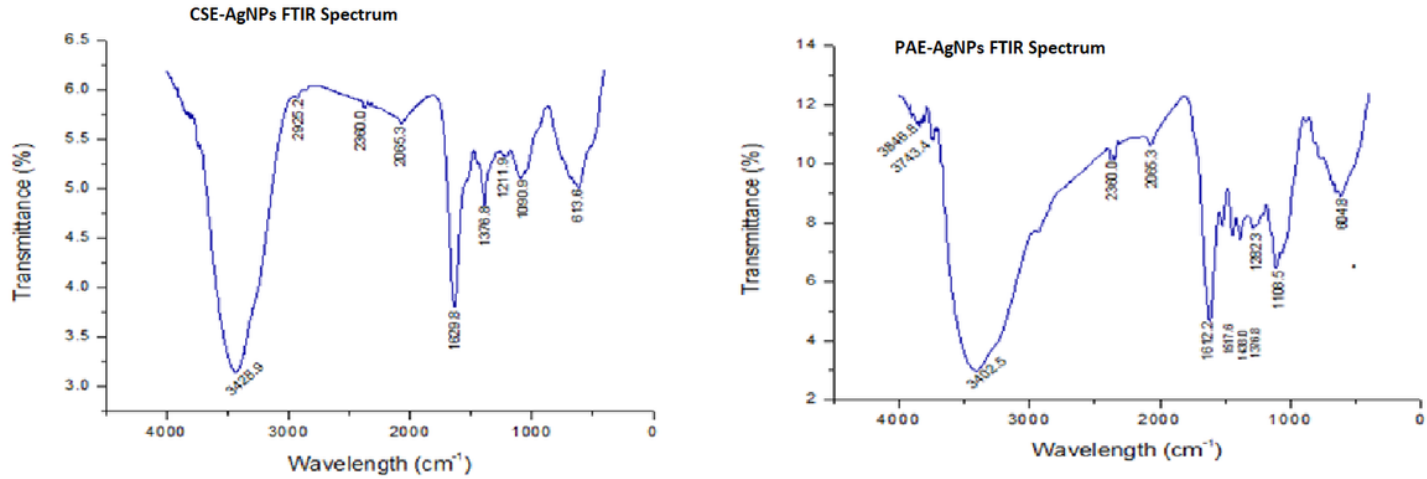

Figure 6

FTIR spectra for biosynthesized AgNPs

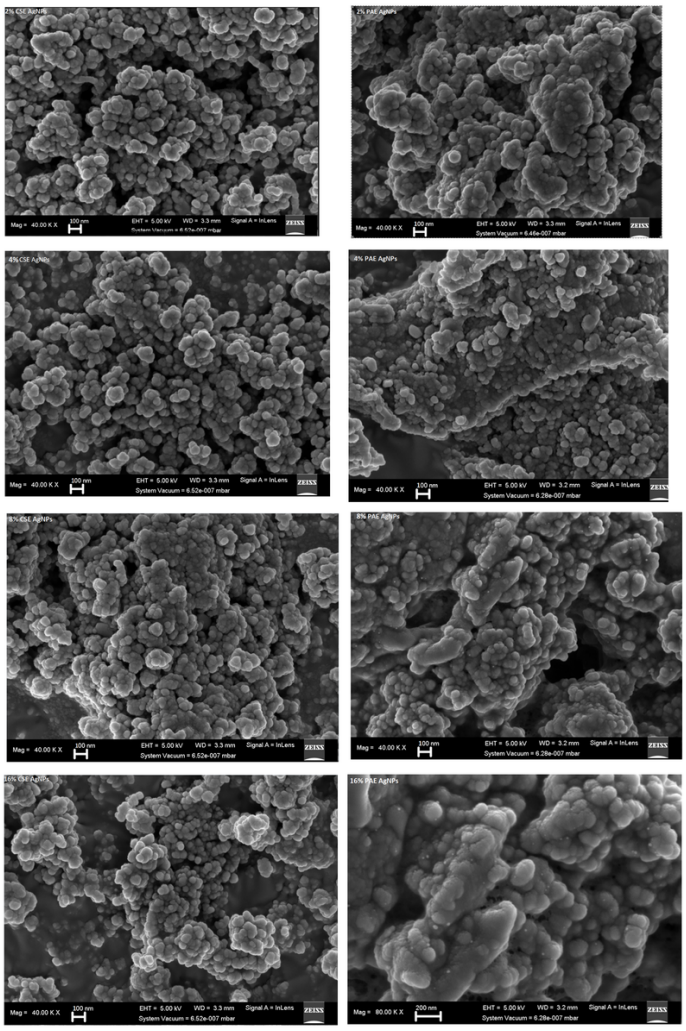

Figure 7

FESEM images of Biosynthesized AgNPs. AgNPs represents Silver nanoparticles, CSE: Camellia sinensis extract and PAE: Prunus africana extract

Supplementary Files

This is a list of supplementary files associated with this preprint. Click to download.

- SNAgNPsSupplTables.docx